# Effects of $Ca^{2+}$, $Mg^{2+}$, and Myristoylation on Guanylyl Cyclase Activating Protein 1 Structure and Stability†

Sunghyuk Lim,‡ Igor Peshenko,§ Alexander Dizhoor,§ and James B. Ames*,‡

*Department of Chemistry, University of California, Davis, California 95616, and Basic Sciences, Pennsylvania College of Optometry, Salus University, Elkins Park, Pennsylvania 19027*

*Received October 8, 2008; Revised Manuscript Received December 17, 2008*

ABSTRACT: Guanylyl cyclase activating protein 1 (GCAP1), a member of the neuronal calcium sensor (NCS) subclass of the calmodulin superfamily, confers $Ca^{2+}$-dependent activation of retinal guanylyl cylcase (RetGC) during phototransduction in vision. Here we analyze the energetics of $Ca^{2+}$ and $Mg^{2+}$ binding to the individual EF-hands, characterize metal-induced conformational changes, and evaluate structural effects of myristoylation as studied by isothermal titration calorimetry (ITC), differential scanning calorimetry (DSC), and nuclear magnetic resonance (NMR). GCAP1 binds cooperatively to $Ca^{2+}$ at EF3 and EF4 ($\Delta H_{EF3} = -3.5$ kcal/mol, and $\Delta H_{EF4} = -0.9$ kcal/mol) with nanomolar affinity ($K_{EF3} = 80$ nM, and $K_{EF4} = 200$ nM), and a third $Ca^{2+}$ binds entropically at EF2 ($\Delta H_{EF2} = 3.1$ kcal/mol, and $K_{EF2} = 0.9$ $\mu$M). GCAP1 binds functionally to $Mg^{2+}$ at EF2 ($\Delta H_{EF2} = 4.3$ kcal/mol, and $K_{EF2} = 0.7$ mM) required for RetGC activation. $Ca^{2+}$ and/or $Mg^{2+}$ binding to GCAP1 dramatically alters DSC and NMR spectra, indicating metal-induced protein conformational changes in EF2, EF3, and EF4. Myristoylation of GCAP1 does not significantly alter its metal binding energetics or NMR spectra, suggesting that myristoylation does not influence the structure of the metal-binding EF-hands. Myristoylation also has almost no effect on protein folding stability measured by DSC. NMR resonances of myristate attached to GCAP1 are exchange-broadened, upfield-shifted, and insensitive to $Ca^{2+}$, consistent with the myristoyl group being sequestered inside the protein as seen in the crystal structure. We conclude that the protein environment near the myristate is not influenced by $Mg^{2+}$ or $Ca^{2+}$ binding but instead is constitutively dynamic and may play a role in promoting interactions of GCAP1 with the cyclase.

Guanylyl cyclase activating proteins (GCAPs) belong to the neuronal calcium sensor (NCS) branch of the calmodulin superfamily (*1*−*3*) and regulate $Ca^{2+}$-sensitive activity of retinal guanylyl cyclase (RetGC)[1] in rod and cone cells (*4, 5*). Phototransduction in retinal rods and cones is modulated by intracellular $Ca^{2+}$ sensed by GCAPs (*6, 7*), and defects in $Ca^{2+}$ signaling by GCAPs are linked to retinal diseases (*8*). Light excitation of photoreceptor cells triggers a phototransduction cascade, leading to the closure of cGMP-gated channels, which hyperpolarizes the plasma membrane and generates a neural signal (*9*). The recovery of the dark state requires activation of RetGC to restore the cytosolic cGMP level. The activity of RetGC is $Ca^{2+}$-sensitive (*10*) and is mediated by GCAPs (*4, 5, 7*). Channel closure during phototransduction blocks the entry of $Ca^{2+}$ and lowers the cytosolic $Ca^{2+}$ concentration from ~250 nM in the dark to ~25 nM in the light (*11*). This drop in $Ca^{2+}$ level causes the formation of $Ca^{2+}$-free and $Mg^{2+}$-bound GCAPs that activate RetGC (*12*), whereas $Ca^{2+}$-bound GCAPs inhibit RetGC at high $Ca^{2+}$ levels generated in the dark (*7*).

The GCAPs [GCAP1 (*5*), GCAP2 (*13*), GCAP3 (*14*), and GCAP4−8 (*15*)] are all ~200-residue proteins containing a covalently attached N-terminal myristoyl group and four EF-hand motifs (Figure 1). $Mg^{2+}$ binds to three EF-hands (EF2, EF3, and EF4) when cytosolic $Ca^{2+}$ levels are low and $Mg^{2+}$-bound GCAP1 activates RetGC (*12, 16*). $Ca^{2+}$ also binds functionally to these three EF-hands (*12, 17*) when $Ca^{2+}$ levels are high in the dark. The first EF-hand (EF1) is unable to bind $Ca^{2+}$ or $Mg^{2+}$ due to conserved substitutions in the binding loop (Cys29 and Pro30 in GCAP1). The X-ray crystal structure of $Ca^{2+}$-bound GCAP1 (*18*) and the NMR structure of GCAP2 (*19*) clearly showed that $Ca^{2+}$ is bound at EF2, EF3, and EF4. In addition, the N-terminal myristoyl group in GCAP1 is buried inside the $Ca^{2+}$-bound protein flanked by hydrophobic residues at the N- and C-termini (see the italicized residues in Figure 1). The structure of the physiologically active form of GCAPs ($Mg^{2+}$-bound and $Ca^{2+}$-free state) is currently unknown.

What are the $Ca^{2+}$- and $Mg^{2+}$-dependent conformational changes in GCAPs that promote activation of RetGC? Recoverin is the only NCS protein whose structure is known

† This work was supported by NIH Grants NS045909, EY012347 (J.B.A.), and RR11973 (University of California, Davis, NMR). A.D. is The Martin and Florence Hafter Chair Professor of Pharmacology.

* To whom correspondence should be addressed. Telephone: (530) 752-6358. Fax: (530) 752-8995. E-mail: ames@chem.ucdavis.edu.

‡ University of California.

§ Salus University.

[1] Abbreviations: $Ca^{2+}$, calcium ion; $Mg^{2+}$, magnesium ion; DSC, differential scanning calorimetry; GCAP1, guanylyl cyclase activating protein 1; EDTA, ethylenediaminetetraacetic acid; HMQC, heteronuclear multiple-quantum coherence; HSQC, heteronuclear single-quantum coherence; IPTG, isopropyl $\beta$-D-1-thiogalactopyranoside; ITC, isothermal titration calorimetry; NMR, nuclear magnetic resonance; NOE, nuclear Overhauser effect; NOESY, nuclear Overhauser effect spectroscopy; RetGC, retinal guanylyl cyclase; SDS−PAGE, sodium dodecyl sulfate−polyacrylamide gel electrophoresis.

10.1021/bi801897p CCC: $40.75 
Published on Web 01/14/2009

```
                1       10                  20        30        40        50
GCAP1           MGNIMDGKSV EEL..... ...SSTECHQ WYKKFMTECP SGQLTLYEFR QFFGLKNLSP
GCAP2           MGQQFSWEEA EE....NGAV GAADAAQLQE WYKKFLEECP SGTLFMHEFK RFFKVPD.NE
GCAP3           MGNGKSIAGD .........Q KAVPTQETHV WYRTFMMEYP SGLQTLHEFK TLLGLQGLNQ
recoverin       MGNSKSGALS KEILEELQLN TKFTEEELSS WYQSFLKECP SGRITRQEFQ TIYSKFFPEA
                                                    EF1

                          60        70        80        90        100       110
GCAP1           WASQYVEQMF ETFDFNKDGY IDFMEYVAAL SLVLKGKVEQ KLRWYFKLYD VDGNGCIDRD
GCAP2           EATQYVEAMF RAFDTNGDNT IDFLEYVAAL NLVLRGTLEH KLKWTFKIYD KDRNGCIDRQ
GCAP3           KANKHIDQVY NTFDTNKDGF IDFLEFIAAV NLIMQEKMEQ KLKWYFKLYD ADGNGSIDKN
recoverin       DPKAYAQHVF RSFDANSDGT LDFKEYVIAL HMTSAGKTNQ KLEWAFSLYD VDGNGTISKN
                             EF2                                        EF3

                         120                 130       140       150       160
GCAP1           ELLTIIRAIR AINP.C.... ....SDSTMT AEEFTDTVFS KIDVNGDGEL SLEEFMEGVQ
GCAP2           ELLDIVESIY KLKKACSVEV EAEQQGKLLT PEEVVDRIFL LVDENGDGQL SLNEFVEGAR
GCAP3           ELLDMFMAVQ ALNG..... .....QQTLS PEEFINLVFH KIDINNDGEL TLEEFINGMA
recoverin       EVLEIVTAIF KMISPEDTKH L...PEDENT PEKRAEKIWG FFGKKDDDKL TEKEFIEGTL
                                                           EF4

                        170       180           190           200
GCAP1           KDQMLLDTLT RSLDLTRIVR RLQNGEQ.DE EGASGR.... ETEAAEADG  204
GCAP2           RDKWVMKMLQ MDLNPSSWIS QQR..... .......... ...RKSAMF  205
GCAP3           KDQDLLEIVY KSFDFSNVLR VICNGKQPDM ETDSSKSPDK AGLGKVKMK  210
recoverin       ANKEILRLIQ FE..PQKVKE K......... .......... ...LKEKKL  202
```

FIGURE 1: Amino acid sequence alignment of GCAP1 with various NCS proteins. Secondary structural elements are indicated schematically. The four EF-hands (EF1, EF2, EF3, and EF4) are underlined. Mutated residues in the EF-hand loops are indicated in bold. N- and C-terminal residues that interact with myristate are shown in italics.

in both the $Ca^{2+}$-free and $Ca^{2+}$-bound states (Figure 1) (*20, 21*). $Ca^{2+}$-free recoverin contains a highly sequested myristoyl group buried inside the protein that interacts intimately with residues from EF1, EF2, and EF3 (*22, 23*). $Ca^{2+}$ binding at EF2 and EF3 leads to large overall conformational changes in recoverin that promote the extrusion of the fatty acyl group outward, enabling it to interact with membrane targets (*20, 24*). Since the target for GCAPs (RetGC) is a membrane protein, we wondered if GCAPs might undergo a similar $Ca^{2+}$-induced conformational change and if $Ca^{2+}$ and/or $Mg^{2+}$ binding to GCAPs alters the protein environment around the myristoyl group. Here, we perform ITC, DSC, and NMR studies on GCAP1 to analyze the thermodynamics of $Ca^{2+}$ and $Mg^{2+}$ binding to the individual EF-hands, characterize metal-induced protein conformational changes, and evaluate the $Ca^{2+}$- and $Mg^{2+}$-dependent structural environment around the myristoyl group.

## EXPERIMENTAL PROCEDURES

*GCAP1 Protein Expression and Purification.* Plasmids (pET11d) encoding wild-type GCAP1 and its mutants for disabling both $Ca^{2+}$ and $Mg^{2+}$ binding [D68G/E75Q (EF2−), D100N/D102G (EF3−), D144N/D148G (EF4−), and D100N/D102G/D144N/D148G (EF34−)] were prepared as described previously (*12*). All plasmids contain the D6S mutation for the recognition of yeast *N*-myristoyltransferase (NMT) needed for expressing recombinant myristoylated GCAP1 in *Escherichia coli*. Plasmid vector (pET11d) harboring GCAP1 or its mutants were cotransformed into BL21(DE3) cells with or without the pBB131 vector encoding NMT. The bacterial cells were typically precultured until the optical density at 600 nm ($A_{600}$) reached 1.0 in 20 mL of Luria-Bertani (LB) medium at 37 °C with antibiotics (100 $\mu$g/mL ampicillin or with 50 $\mu$g/mL kanamycin). They were then inoculated into 1 L of LB medium with the antibiotics and grown until the $A_{600}$ reached 1.3. GCAP1 and NMT proteins were coexpressed upon addition of isopropyl $\beta$-D-1-thiogalactopyranoside (IPTG) to the cell culture to a final concentration of 0.5 mM at 25 or 37 °C for 4−16 h. GCAP1 was expressed either in the soluble fraction or as inclusion bodies by adjusting the induction temperature: Soluble GCAP1 expression occurs at 25 °C, whereas GCAP1 expression in inclusion bodies occurred at 37 °C. For the expression of myristoylated proteins, 5 mg/L (final concentration) myristic acid (from a 5 mg/mL ethanol stock) was added to the culture 20 min prior to the induction. The purification of myristoylated GCAP1 and mutants (EF2−, EF3−, EF4−, and EF34−) expressed in inclusion bodies has been described previously (*12*).

The purification of recombinant unmyristoylated GCAP1 (expressed in soluble lysate) was as follows. Cells were harvested by centrifugation, and the cell pellet was resuspended and sonicated in lysis buffer containing 20 mM Tris-HCl (pH 7.5), 0.1 M KCl, 2 mM EGTA, 1 mM DTT, 10% glycerol, and 0.1 mM PMSF. The cell lysate was centrifuged at 100000*g* by ultracentrifugation. The supernatant was mixed with $CaCl_2$ to a final concentration of 3 mM and then applied onto a butyl-Sepharose column (HiPrep 16/10 Butyl FF, Amersham) which was pre-equilibrated with buffer A containing 20 mM Tris (pH 7.5), 0.3 M KCl, 2 mM $CaCl_2$, 1 mM $MgCl_2$, and 1 mM DTT. The elution of the protein was conducted via removal of $Ca^{2+}$ ions via addition of buffer B containing 20 mM Tris (pH 7.5), 0.1 M KCl, 2 mM EGTA, and 1 mM DTT. The fractions containing target proteins were pooled and diluted 3-fold with $ddH_2O$, lowering the ionic strength for anion exchange column application. For myristoylated GCAP1, a similar purification procedure was followed except that the lysis buffer contained 0.5 M ammonium sulfate instead of 0.1 M KCl. This modification was necessary to cause more efficient binding and elution of myristoylated GCAP1 using butyl-Sepharose chromatography. GCAP1 protein samples were then further

purified by DEAE anion exchange chromatography (HiTrap 5 mL DEAE FF, Amersham) pre-equilibrated with 20 mM Tris (pH 7.5) buffer containing 1 mM EGTA and 1 mM DTT. GCAP1 was eluted using a linear NaCl gradient (from 0 to 0.5 M over 20 column volumes). Lastly, proteins were purified with a size-exclusion chromatography column (HiLoad 26/60 Superdex 200, Amersham) pre-equilibrated with 20 mM Tris (pH 7.5) buffer containing 1 mM EGTA and 1 mM DTT. The final purity (>95%) of the GCAP1 sample was verified by SDS−PAGE and mass spectrometry.

Metal-free GCAP1 was prepared as described previously (*16*). Briefly, the final purified GCAP1 samples in the presence of 5 mM EGTA were concentrated 10-fold (Amicon-10, 10 kDa cutoff), diluted 10-fold with decalcified buffer [prepared as described previously (*25, 26*)], and then concentrated again. This procedure was repeated four times to completely exchange GCAP1 into decalcified and EGTA-free buffer used in the metal binding studies. The free $Ca^{2+}$ concentration in the apo-GCAP1 sample was verified to be less than 10 nM using fluo-3 flourescent indicator dye analysis (*27*) and atomic absorption measurements. The lack of $Ca^{2+}$ in apo-GCAP1 was also verified by monitoring the absence of downfield-shifted amide proton NMR resonances of Gly69, Gly105, and Gly149 that report on $Ca^{2+}$ binding to EF2, EF3, and EF4, respectively. The apo-GCAP1 samples were also shown by NMR not to contain any lingering EGTA.

*Isothermal Titration Calorimetry (ITC).* All ITC experiments were performed using a VP-ITC calorimeter (MicroCal), and the data were processed with Origin 7 from MicroCal as described previously (*28*). GCAP1 samples (myristoylated, unmyristoylated, wild type, and mutants) for ITC studies were prepared in 20 mM Tris buffer (pH 7.5), 100 mM NaCl, and 1 mM $\beta$-mercaptoethanol. The protein concentration was either 25 or 50 $\mu$M and was determined by measuring the optical density at 280 nm. A series of 5 $\mu$L aliquots of 2 mM $CaCl_2$ were injected into the protein sample (1.6 mL) in the presence and absence of 2 mM $Mg^{2+}$, and corresponding heat signals were monitored calorimetrically. For the $Mg^{2+}$ titration, 10 $\mu$L aliquots of 40 mM $MgCl_2$ were titrated into the protein sample. All titrations were typically performed at 30 °C. Additional titrations were also performed at 23, 25, and 27 °C for measuring $\Delta C_p$ (*29, 30*). The baseline from a buffer blank titration was subtracted from the raw data. A sequential binding sites model was used to fit ITC data using a nonlinear least-squares minimization method (*31*) and calculate the dissociation constant ($K_d$) and enthalpy change ($\Delta H$) for each site.

*Fluorescence.* Tryptophan fluorescence emission spectra of myrGCAP1 were observed with a Varian Cary Eclipse spectrometer. Protein samples were prepared in 20 mM Tris-HCl (pH 7.5) buffer containing 5 mM DTT in a 1 cm path length cell with increasing amounts of guanidine HCl (0−6 M) in the presence and absence of 5 mM $Ca^{2+}$ or $Mg^{2+}$. The protein concentration was 10 $\mu$M. The emission spectra were recorded in range of 300−500 nm with the excitation wavelength set at 295 nm at room temperature. The protein samples were incubated at room temperature for 30 min before each measurement.

*NMR Spectroscopy.* For $^1H-^{15}N$ HSQC experiments, samples of myristoylated and unmyristoylated GCAP1 were prepared in 5 mM Tris-$d_{11}$-HCl (pH7.4) buffer containing 10% $D_2O$, 1 mM dithiothreitol-$d_{10}$ (DTT), and either 5 mM $CaCl_2$ or 5 mM $MgCl_2$. For $^1H-^{13}C$ HMQC experiments, NMR samples were prepared under conditions similar to those described above except the sample was prepared in 100% $D_2O$. The reading of the pH meter was not corrected for the deuterium isotope effect. The sample concentration was typically around 0.3 mM.

All NMR spectra were recorded using a Bruker Advance 600 MHz spectrometer equipped with a triple-resonance cryo-probe and z gradient. Typically, spectra were recorded at 300, 310, and 320 K with 8−32 scans per increment. For $^{15}N$-labeled myristoylated GCAP1 (apo, $Mg^{2+}$-bound, or $Ca^{2+}$-bound form), two-dimensional (2D) $^1H-^{15}N$ HSQC spectra with a total of 256 increments were acquired. For samples of GCAP1 with the $^{13}C$-labeled myristic group covalently attached to the N-terminus, 2D $^1H-^{13}C$ HMQC spectra were recorded with 1024 × 256 points. Three dimensional ($^{13}C$/F1)-edited $^{13}C$/F3-filtered HMQC-NOESY spectra (mixing time of 120 ms) were obtained with 1024 × 64 × 180 points (*23, 32*).

*Differential Scanning Calorimetry.* A VP-DSC calorimeter from MicroCal was used for all DSC measurements, and the data were processed with Origin 7 from MicroCal as described previously (*28*). Scanning was done in the temperature range of 10−120 °C at a scan rate of 60 °C/h. A buffer baseline was subtracted from each scan. Myristoylated and unmyristoylated GCAP1 at concentrations of 50 $\mu$M were prepared in 20 mM Tris buffer (pH 7.5) containing 100 mM NaCl and 1 mM $\beta$-mercaptoethanol with or without 2 mM $CaCl_2$ or $MgCl_2$. Samples were degassed before each scan.

## RESULTS

*Thermodynamics of $Ca^{2+}$ Binding to GCAP1.* Isothermal titration calorimetry (ITC) was used in this study to analyze the energetics of $Ca^{2+}$ and $Mg^{2+}$ binding to the individual EF-hands of GCAP1 (Figure 1). Previous equilibrium binding studies revealed that GCAP1 binds $Ca^{2+}$ at EF2, EF3, and EF4 in the nanomolar range (*16*), but precise values of dissociation constants for the individual EF-hands were difficult to resolve because their binding appeared to be somewhat overlapped. ITC can resolve dissociation constants ($K_d$) of multiple sites on the basis of differences in their binding enthalpy ($\Delta H$). Hence, two or more sites with similar dissociation constants can be resolved if their binding enthalpies are sufficiently different or vice versa.

The $Ca^{2+}$ binding properties of both myristoylated and unmyristoylated GCAP1 were monitored by ITC (Figure 2). N-Terminal myristoylation of GCAP1 had a very small influence on $Ca^{2+}$ binding (see the circles in Figure 2A,B) unlike that of recoverin (*26, 33*), and all subsequent analyses below were performed on myristoylated GCAP1. Titration of $CaCl_2$ into myristoylated GCAP1 resulted in a binding isotherm that is multiphasic and best fit by a three-site sequential binding model (solid lines in Figure 2A,B and Table 1), consistent with $Ca^{2+}$ binding at EF2, EF3, and EF4 as suggested by previous fluorescence equilibrium binding studies (*12, 16*). The ITC $Ca^{2+}$ binding isotherm of apo-GCAP1 (without $Mg^{2+}$; see Figure 2A) exhibited exothermic binding of two $Ca^{2+}$ ($\Delta H_1 = -3.5$ kcal/mol, and $\Delta H_2 = -0.9$ kcal/mol) in the nanomolar range followed by endo-

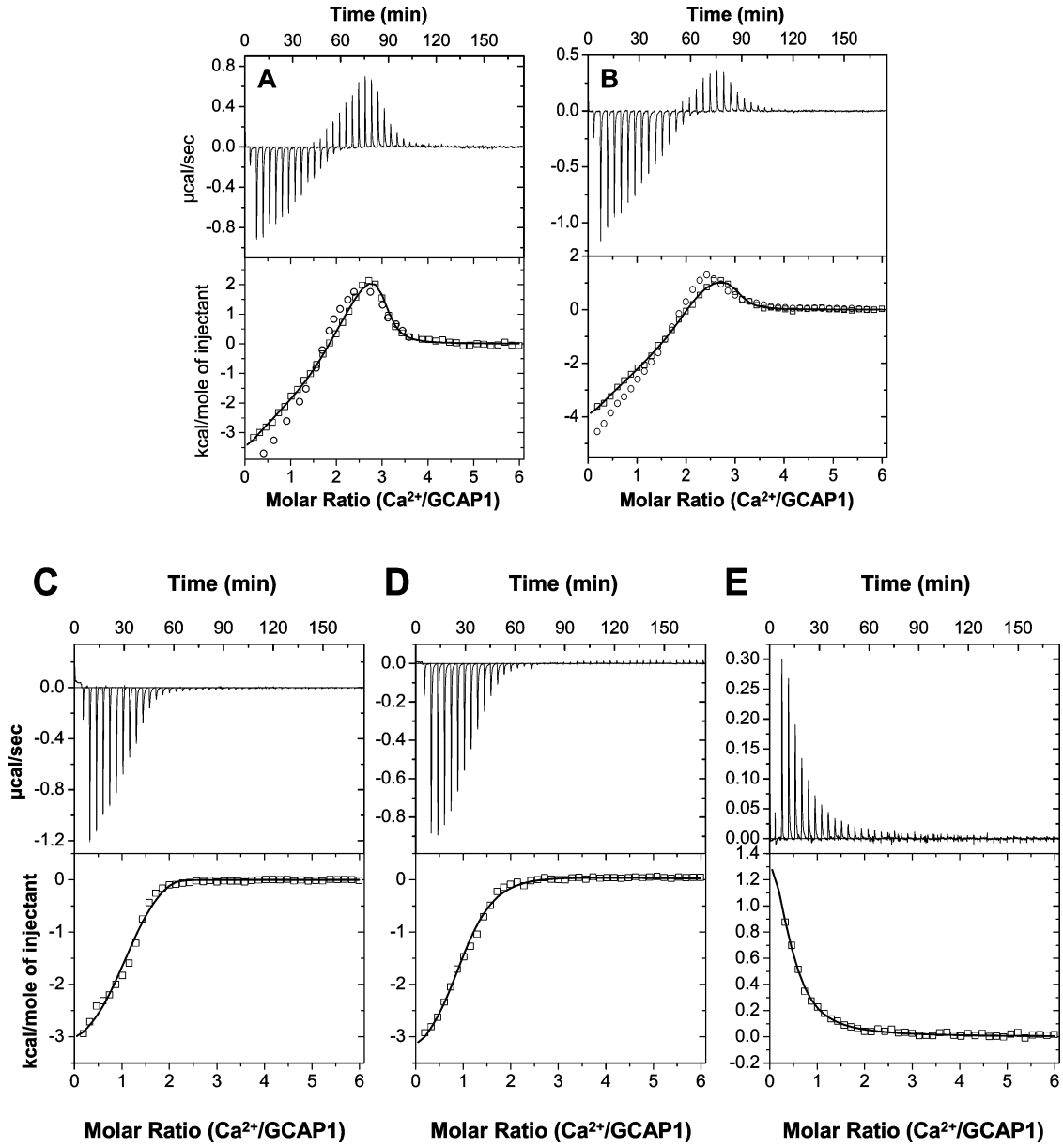


FIGURE 2: ITC $Ca^{2+}$ titration of apo-GCAP1$^{WT}$ (A), $Mg^{2+}$-bound GCAP1$^{WT}$ (B), apo-EF2− (C), apo-EF4− (D), and apo-EF34− (E). The top panels show representative scans of ITC data from the $Ca^{2+}$ titrations. The bottom panels show plots of the corresponding integrated binding isotherms fit to a sequential binding model with three sites (wild type), two sites (EF2− and EF4−), or one site (EF34−) as described in Experimental Procedures (—). Optimal fitting parameters are listed in Table 1. $Ca^{2+}$ binding isotherms of unmyristoylated GCAP1 are overlaid (○) in panels A and B.

Table 1: Thermodynamic Parameters of $Ca^{2+}$ Binding to GCAP1 and Mutants at 30 °C[a]

| | $K_{EF2}$ | $K_{EF3}$ | $K_{EF4}$ | $\Delta H_{EF2}$ | $\Delta H_{EF3}$ | $\Delta H_{EF4}$ |
|---|---|---|---|---|---|---|
| | | | No $Mg^{2+}$ | | | |
| wild type | 0.9 ± 0.2 | 0.08 ± 0.05 | 0.2 ± 0.05 | 3.1 ± 0.1 | −3.5 ± 0.1 | −0.9 ± 0.2 |
| EF2− | − | 0.2 ± 0.1 | 0.7 ± 0.5 | − | −3.0 ± 0.1 | −0.05 ± 0.1 |
| EF4− | 69 ± 20 | 4.9 ± 0.9 | − | 0.8 ± 0.1 | −3.4 ± 0.1 | − |
| EF34− | 11 ± 1 | − | − | 2.1 ± 0.2 | − | − |
| | | | 2 mM $Mg^{2+}$ | | | |
| wild type | 1.6 ± 0.3 | 0.1 ± 0.05 | 0.2 ± 0.05 | 1.4 ± 0.1 | −3.9 ± 0.1 | −0.6 ± 0.2 |
| EF2− | − | 0.2 ± 0.1 | 2.0 ± 0.4 | − | −4.2 ± 0.1 | −0.5 ± 0.2 |
| EF4− | 1.1 ± 0.2 | 0.4 ± 0.1 | − | 0.4 ± 0.1 | −4.0 ± 0.1 | − |
| EF34− | 50 ± 20 | − | − | 1.6 ± 0.1 | − | − |

[a] Dissociation constants ($K_{EF2}$, $K_{EF3}$, and $K_{EF4}$) are expressed in micromolar, and the enthalpy differences ($\Delta H_{EF2}$, $\Delta H_{EF3}$, and $\Delta H_{EF4}$) are expressed in kilocalories per mole.

thermic binding of one $Ca^{2+}$ ($\Delta H$ = 3.1 kcal/mol) with a much lower affinity ($K_d$ = 0.9 $\mu$M). The high-resolution ITC data clearly indicated three binding sites having distinct values of $\Delta H$ and $K_d$. To assign each ITC binding phase as binding by a particular EF-hand, we have constructed various mutants that disable functional $Ca^{2+}$ binding to the individual

EF-hands (Figure 1): D68G/E75Q (EF2−), D100N/D102G (EF3−), D144N/D148G (EF4−), and D100N/D102G/D144N/D148G (EF34−). In each mutant, a negatively charged Glu or Asp at the beginning and end of the EF-hand loop has been substituted with a neutral residue (Gln or Asn). Also, the second negatively charged residue in the loop (Asp) was replaced with Gly. These substitutions dramatically lower the $Ca^{2+}$ and/or $Mg^{2+}$ binding affinity of the respective EF-hand outside of the physiological range as previously described in detail (*16, 34*).

The ITC isotherms for wild-type GCAP1 and each of the EF-hand mutants were fit to a sequential binding model (solid lines in Figure 2), and optimal $Ca^{2+}$ binding parameters ($\Delta H$ and $K_d$) are listed in Table 1. All ITC $Ca^{2+}$ binding measurements were performed both in the presence (Figure 2B) and in the absence (Figure 2A) of physiological $Mg^{2+}$ levels (2 mM $Mg^{2+}$) at 30 °C. We show that $Mg^{2+}$ has relatively small effects on $Ca^{2+}$ binding, indicating that GCAP1 binds selectively to $Ca^{2+}$ with an at least 500-fold preference over $Mg^{2+}$ (Table 1). The ITC $Ca^{2+}$ binding isotherm of the EF2− mutant (Figure 2C) exhibited exothermic binding of two $Ca^{2+}$ but lacked the endothermic phase seen in the wild type, indicating that EF2 must be the low-affinity endothermic site. Correspondingly, the ITC isotherm of EF34− (Figure 2E) exhibited only endothermic binding ($\Delta H = 2.1$ kcal/mol), further confirming that EF2 is the endothermic site. The ITC $Ca^{2+}$ binding isotherm of EF4− (Figure 2D) exhibited an exothermic phase ($\Delta H = -3.4$ kcal/mol) assigned as $Ca^{2+}$ binding at EF3 followed by a lower-affinity, endothermic phase ($K_d = 69$ $\mu$M, and $\Delta H = 0.8$ kcal/mol) assigned above to EF2. By the process of elimination, the lower-affinity exothermic site in the wild-type isotherm ($\Delta H = -0.9$ kcal/mol, and $K_d = 200$ nM), therefore, must be assigned to EF4.

Our ITC $Ca^{2+}$ binding analysis summarized in Table 1 reveals that EF2 is an endothermic site ($K_{EF2} = 0.9$ $\mu$M, and $\Delta H_{EF2} = 3.1$ kcal/mol); EF3 and EF4 exhibit exothermic binding in the nanomolar range ($K_{EF3} = 80$ nM, and $\Delta H_{EF3} = -3.5$ kcal/mol; $K_{EF4} = 200$ nM, and $\Delta H_{EF4} = -0.9$ kcal/mol). The $Ca^{2+}$ binding dissociation constants of EF3 and EF4 are in the physiological range of free $Ca^{2+}$ concentration measured in rod outer segments (*11*) and are similar to binding constants measured previously by direct equilibrium $Ca^{2+}$ binding assays (*12, 16*). The relatively low apparent $Ca^{2+}$ binding affinity of EF2 measured by ITC ($K_{EF2} = 0.9$ $\mu$M) is ~10-fold weaker than the intrinsic binding affinity determined by fluorescence $Ca^{2+}$ binding assays (*16*). The discrepancy is explained in part by a protein conformational change in GCAP1 that is thermodynamically coupled to $Ca^{2+}$ binding at EF2. The intrinsic $Ca^{2+}$ binding at EF2 measured by the fluorescence binding assay ($K_a = 10^7$ $M^{-1}$) coupled to an unfavorable conformational change ($K_{eq} \sim 10^{-1}$) probed by ITC yields an overall equilibrium constant of $K_{tot}$ ($=K_aK_{eq} \sim 10^6$ $M^{-1}$), consistent with the overall $K_d$ measured by ITC. Hence, the overall low apparent binding affinity of EF2 suggests that $Ca^{2+}$ binding at this site drives an unfavorable protein conformational change. Consistent with this conformational change are large $Ca^{2+}$-induced NMR chemical shift changes for residues in EF2 (see below) and the relatively steep temperature dependence of $\Delta H_{EF2}$ ($\Delta C_p = -139$ cal $mol^{-1}$ $K^{-1}$), suggesting a change in the solvent accessible hydrophobic surface area caused by $Ca^{2+}$ binding at EF2 (*29, 30*).

$Ca^{2+}$-induced conformational changes in EF2 are further supported by its $Mg^{2+}$-dependent $Ca^{2+}$ binding properties. Physiological $Mg^{2+}$ levels [~1 mM in rod outer segments (*35*)] are required for GCAP1 to activate RetGC at low $Ca^{2+}$ levels, implying that $Ca^{2+}$-free GCAP1 must bind $Mg^{2+}$ (see below) (*16*). The presence of physiological $Mg^{2+}$ levels caused an ~1.8-fold increase in $K_{EF2}$ and a 2-fold decrease in $\Delta H_{EF2}$, with smaller effects on binding to EF3 and EF4 (Table 1). This suggests that $Mg^{2+}$ competes with $Ca^{2+}$ for binding at EF2 even at high $Ca^{2+}$ concentrations (~1 $\mu$M in dark-adaped rods), but $Mg^{2+}$ does not effectively compete for binding at EF3 and EF4 under these conditions. We conclude that both $Mg^{2+}$- and $Ca^{2+}$-induced conformational changes in EF2 are consistent with recent studies showing that binding of GCAP1 to RetGC requires $Mg^{2+}$ binding to EF2 under conditions that mimic light adaptation of rods (*12, 17*).

We do not see any evidence of $Ca^{2+}$ binding at EF1. The primary structure of EF1 contains unfavorable substitutions (e.g., Cys29 and Pro30 in Figure 1) known to abolish physiological $Ca^{2+}$ binding at this site in other NCS proteins (*3, 36, 37*). Accordingly, our ITC $Ca^{2+}$ binding measurements on GCAP1 do not detect any heat signal from $Ca^{2+}$ binding at EF1, suggesting that either EF1 does not bind $Ca^{2+}$ under physiological conditions or the enthalpy of binding is zero.

*$Mg^{2+}$ Binding to GCAP1.* The presence of physiological levels of $Mg^{2+}$ (2 mM $Mg^{2+}$) is required for activation of RetGC by GCAP1 at low $Ca^{2+}$ levels (*16*), suggesting that $Mg^{2+}$ binds to $Ca^{2+}$-free GCAP1. Indeed, we showed the $Ca^{2+}$ binding affinity of EF2 is $Mg^{2+}$-dependent (Table 1). These $Mg^{2+}$-dependent effects prompted us to quantitate the direct $Mg^{2+}$ binding to GCAP1 using ITC. Titration of $MgCl_2$ into apo-GCAP1 resulted in a biphasic binding isotherm best fit by a sequential two-site model (solid lines in Figure 3A). The binding isotherm shows endothermic $Mg^{2+}$ binding with a high micromolar affinity ($\Delta H = 4.3$ kcal/mol, and $K_d = 700$ $\mu$M) followed by weaker binding in the millimolar range ($\Delta H_{low} = 0.9$ kcal/mol, and $K_{low} = 2$ mM). $Mg^{2+}$ binding experiments were also performed on the EF-hand mutants to assign each $Mg^{2+}$ binding phase.

The ITC isotherms for wild-type and the EF-hand mutants were fit to a sequential binding model (solid lines in Figure 3), and optimal $Mg^{2+}$ binding parameters ($\Delta H$ and $K_d$) are listed in Table 2. The ITC $Mg^{2+}$ binding isotherm of EF34− (Figure 3D) exhibits a single endothermic phase representing binding of $Mg^{2+}$ with high micromolar affinity, suggesting that EF2 must be the highest-affinity endothermic site ($\Delta H_{EF2} = 4.3$ kcal/mol, and $K_{EF2} = 0.7$ mM). Correspondingly, the isotherm of EF2− (Figure 3B) exhibits millimolar binding of one or more $Mg^{2+}$ but lacks the micromolar phase seen in the wild-type isotherm, confirming that EF2 is the highest-affinity site. The lower-affinity endothermic phase in the wild-type isotherm likely represents $Mg^{2+}$ binding to EF3 and/or EF4. However, individual values of $\Delta H$ and $K_d$ for $Mg^{2+}$ binding at EF3 and EF4 could not be accurately resolved due to their low-affinity and nonstoichiometric binding ($K_d \gg$ protein concentration).

Our ITC $Mg^{2+}$ binding analysis reveals that EF2 is an endothermic site with submillimolar affinity ($K_{EF2} = 0.7$ mM,

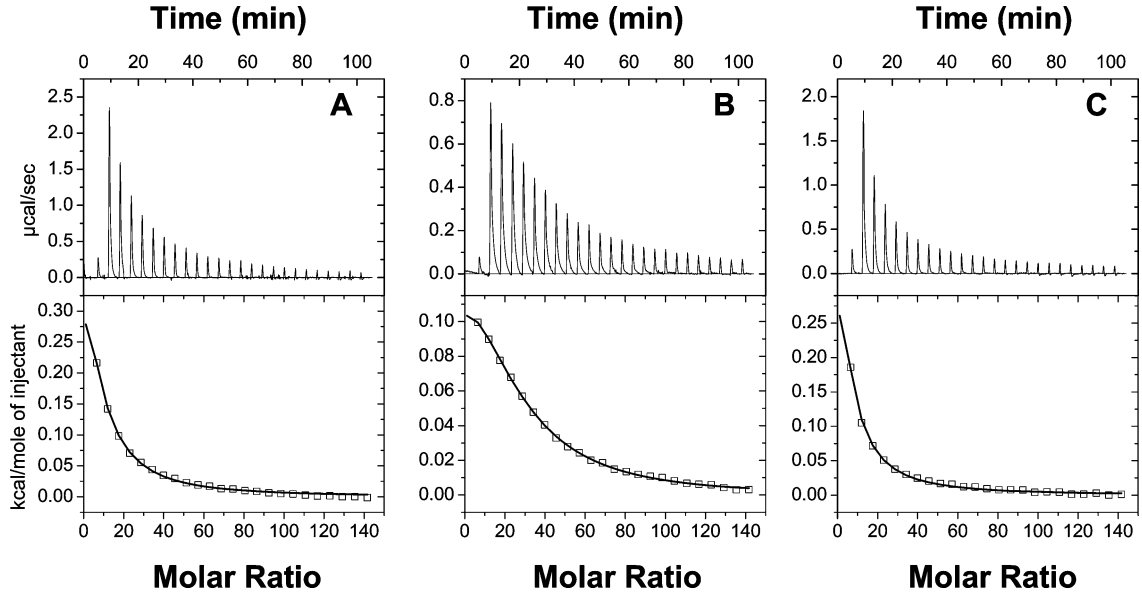


FIGURE 3: ITC $Mg^{2+}$ titration of myristoylated $GCAP1^{WT}$ (A), EF2− (B), and EF34− (C). The top panels show representative scans of ITC data from the $Mg^{2+}$ titrations. The bottom panels show integrated binding isotherms fit to a two-site (WT) or one-site (EF2− and EF34−) model as described in Experimental Procedures (—). Optimal fitting parameters are listed in Table 2.

Table 2: Thermodynamic Parameters of $Mg^{2+}$ Binding to GCAP1 and Mutants at 30 °C[a]

| | $K_{EF2}$ | $K_{low}$ | $\Delta H_{EF2}$ | $\Delta H_{low}$ |
|---|---|---|---|---|
| wild type | 0.7 ± 0.2 | 2 ± 0.8 | 4.3 ± 0.1 | 0.9 ± 0.5 |
| EF2− | − | 2 ± 0.8 | − | 2.9 ± 0.2 |
| EF4− | 0.7 ± 0.2 | 2 ± 0.8 | 0.5 ± 0.3 | 3.9 ± 0.3 |
| EF34− | 0.7 ± 0.2 | − | 4.2 ± 0.1 | − |

[a] Dissociation constants ($K_{EF2}$ and $K_{low}$, low-affinity phase) are expressed in millimolar. The enthalpy differences ($\Delta H_{EF2}$ and $\Delta H_{low}$) are expressed in kilocalories per mole.

and $\Delta H_{EF2}$ = 4.3 kcal/mol); EF3 and/or EF4 binds $Mg^{2+}$ in the millimolar range. $Mg^{2+}$ competes somewhat with $Ca^{2+}$ for binding at EF2, explaining its $Mg^{2+}$-dependent $Ca^{2+}$ binding affinity and enthalpy (Table 1). By contrast, EF3 and EF4 each bind $Ca^{2+}$ with affinities at least 10000-fold higher than that of $Mg^{2+}$, explaining why these sites are more selective for $Ca^{2+}$ and less sensitive to $Mg^{2+}$. $Mg^{2+}$ binding at EF2 may be functionally important and explain why the activation of RetGC by $Ca^{2+}$-free GCAP1 requires physiological levels of $Mg^{2+}$. Indeed, recent experiments have shown that apo-GCAP1 does not regulate RetGC, and $Mg^{2+}$ binding at EF2 is required for light-dependent activation of the cyclase (*17*).

*Folding Stability versus $Ca^{2+}$, $Mg^{2+}$, and Myristoylation.* Differential scanning calorimetry (DSC) experiments were performed on GCAP1 to quantitatively assess the effect of $Ca^{2+}$, $Mg^{2+}$, and myristoylation on protein folding stability. Representative DSC scans of GCAP1 are shown in Figure 4. The peak maximum of unmyristoylated metal-free (apo) GCAP1 (transitition temperature, $T_m$ = 47 °C) is lower than the peak maximum of $Mg^{2+}$-bound ($T_m$ = 55 °C) and $Ca^{2+}$-bound ($T_m$ = 104 °C) unmyristoylated GCAP1, indicating that both $Mg^{2+}$ and particularly $Ca^{2+}$ increase the folding stability quite substantially. N-Terminal myristoylation of GCAP1 has a much smaller effect on the folding stability. The DSC peak maxima of myristoylated GCAP1 in the apo (transition temperature, $T_m$ = 52 °C), $Mg^{2+}$-bound ($T_m$ = 58 °C), and $Ca^{2+}$-bound ($T_m$ = 103 °C) forms are slightly higher than the corresponding melting temperatures of unmyristoylated GCAP1, indicating that myristoylated and unmyristoylated forms of GCAP1 have similar folding stabilities (Figure 4). The transition peaks in all the thermograms did not fully reappear upon rescanning each of the samples, suggesting irreversible unfolding due to aggregation and/or denaturation. In addition, the DSC thermograms of apo-GCAP1, $Mg^{2+}$-bound GCAP1, and $Ca^{2+}$-bound GCAP1 were all quite broad with steeply sloped post-transitional baselines, making it impossible to accurately fit these thermograms by any quantitative models. The cause of the sloping and highly curved baselines is not fully understood but may be explained in part by visible protein aggregation that occurred during unfolding at the very high melting temperatures.

In summary, the DSC analysis on GCAP1 reveals that $Mg^{2+}$ binding and $Ca^{2+}$ binding both increase the protein folding stability. N-Terminal myristoylation of GCAP1 also stabilizes the protein fold slightly as expected on the basis of the sequestered myristoyl group observed in the X-ray crystal structure (*18*). However, the increased folding stability conferred by myristoylation of GCAP1 is much smaller than that observed by myristoylated recoverin (Figure 1 of the Supporting Information). We suggest that the vast majority of the folding stability in GCAP1 is derived by structural interactions among the EF-hands, which would explain the strong dependence of $T_m$ on $Mg^{2+}$ and $Ca^{2+}$ binding. Therefore, the interaction of the myristoyl group with the N- and C-terminal helices observed in the crystal structure appears to contribute very little to the overall protein stability. By contrast, the myristoyl group in $Ca^{2+}$-free recoverin interacts intimately with hydrophobic residues in EF1, EF2, and EF3 (*22*), which explains how $Ca^{2+}$ binding is coupled to extrusion of the myristoyl group and why myristoylation of recoverin has a much more dramatic effect on the overall protein folding stability.

*$Mg^{2+}$ and $Ca^{2+}$ Alter the Tertiary Structure of GCAP1.* NMR spectroscopy was used to probe protein conformational changes in GCAP1 induced by $Mg^{2+}$ and/or $Ca^{2+}$ binding (Figure 5). The peaks in the $^1H-^{15}N$ HSQC NMR spectra

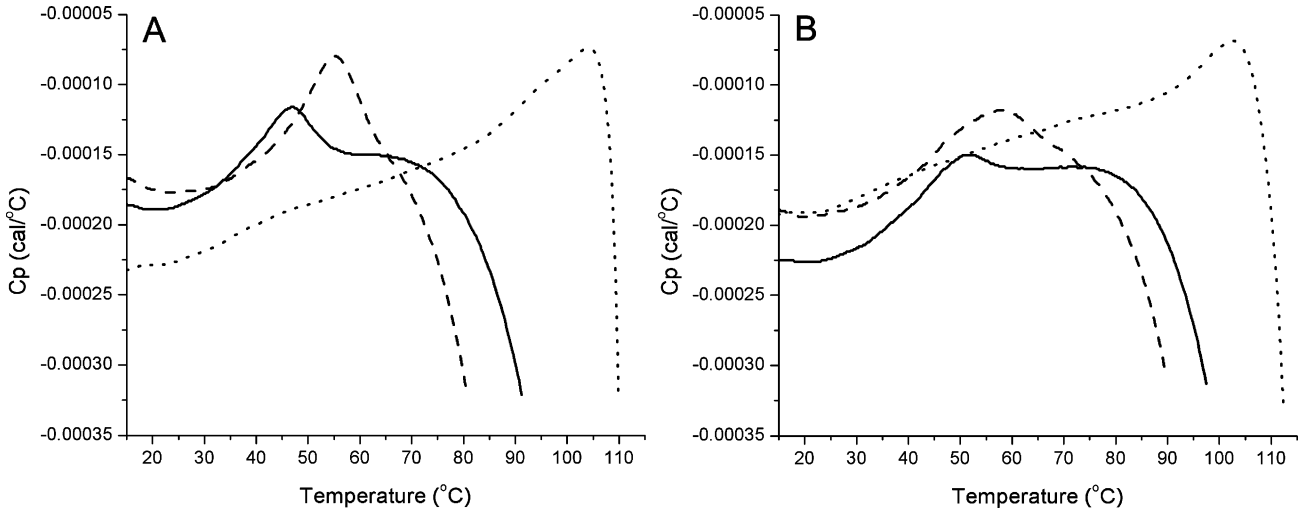


FIGURE 4: DSC scans showing thermal denaturation of GCAP1. Data were obtained for unmyristoylated GCAP1 (A) and myristoylated GCAP1 (B). Thermograms of apo-GCAP1, $Mg^{2+}$-bound GCAP1, and $Ca^{2+}$-bound GCAP1 are represented by solid, dashed, and dotted lines, respectively.

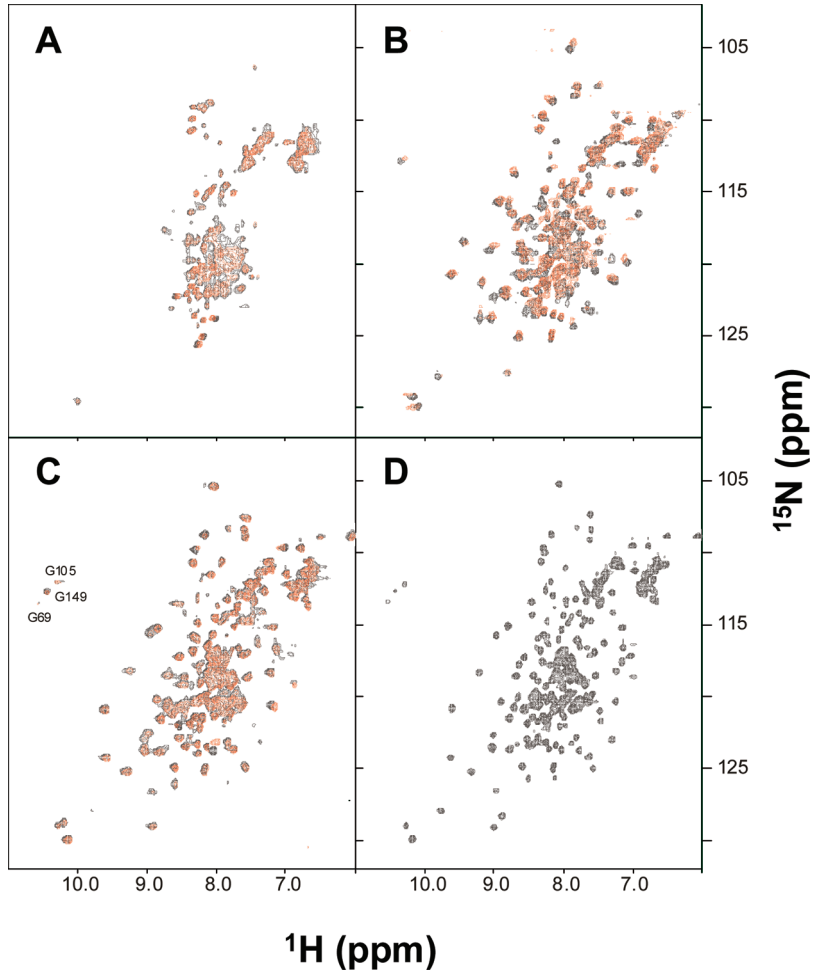


FIGURE 5: NMR spectra of myristoylated and unmyristoylated GCAP1. Two-dimensional ($^{1}H-^{15}N$ HSQC) NMR spectra of $^{15}N$-labeled unmyristoylated (black) and myristoylated GCAP1 (red) in the apo (A), $Mg^{2+}$-bound (B), $Ca^{2+}$-bound (C), and detergent-solubilized, $Ca^{2+}$-bound (D) states. Spectra in panels A−C were recorded at 37 °C, and the spectrum in panel D was recorded in the presence of 25 mM octyl glucoside at 47 °C.

of GCAP1 represent main chain and side chain amide groups and provide a residue-specific fingerprint of the overall protein conformation. HSQC spectra of myristoylated (red) and unmyristoylated (black) forms of GCAP1 look very similar, indicating once again that myristoylation has very little effect on the overall main chain structure of GCAP1. The structural similarity between myristoylated and unmyristoylated GCAP1 is also supported by tryptophan fluorescence emission spectra that have nearly the same emission wavelength maxima (Figure 2 of the Supporting Information). This is in stark contrast to the spectral properties of $Ca^{2+}$-free myristoylated recoverin, in which myristoylation has a

profound influence on both NMR and fluorescence spectra (*32, 33*). The myristoyl group of recoverin interacts intimately with the various EF-hands and induces large overall structural changes in the protein (*20*). By contrast, the myristoyl group of GCAP1 appears to have very little effect on the overall protein structure.

The two-dimensional $^{1}H-^{15}N$ HSQC spectrum of apo-GCAP1 (both myristoylated and unmyristoylated) exhibited poorly resolved and overlapping peaks with narrow chemical shift dispersion in the amide proton dimension (Figure 5A). The number of observed peaks was far smaller than the expected number of amide groups, and the intensities of many peaks were quite weak due to broadening caused by dimerization or conformational heterogeneity. The poor chemical shift dispersion suggests that apo-GCAP1 may form an unstructured molten globule state similar to that described for the apo states of many other $Ca^{2+}$-binding proteins such as GCAP-2 (*19*), Frq1 (*38*), CIB (*39*), calexcitin (*40*), protein S (*41*), and DREAM (*25*). However, circular dichroism analysis (data not shown) suggests that apo-GCAP1 adopts a high degree of helical content, consistent with the formation of the four EF-hands, and that the helical content does not change much upon binding $Mg^{2+}$ and/or $Ca^{2+}$. Together, our structural studies suggest that apo-GCAP1 forms native secondary structure but lacks stable tertiary structure.

The HSQC spectrum of GCAP1 changed upon the addition of a saturating amount of $Mg^{2+}$ (Figure 5B). $Mg^{2+}$ caused a greater number of peaks to appear, and the NMR intensities were in general more uniform than those of apo-GCAP1. $Mg^{2+}$ binding to GCAP1 increased the degree of NMR chemical shift dispersion and increased the number of observable long-range NOEs, demonstrating that $Mg^{2+}$-bound GCAP1 adopts stable tertiary structure. Unfortunately, the number of observable HSQC peaks for $Mg^{2+}$-bound GCAP1 was still only ~50% of the expected number of amide groups, making it impossible to obtain enough sequence-specific assignments necessary to determine the structure by NMR. Also, the average peak width in the spectrum appears much broader than expected for a monomeric protein, consistent with protein dimerization in the NMR samples as determined by size-exclusion chromatography studies (SEC). Pulsed-field gradient diffusion NMR studies (*42*) determined a hydrodynamic radius of 4.0 nm (corresponding to a spherical molecular mass of ~60 kDa) for $Mg^{2+}$-bound GCAP1, consistent with mostly dimer or higher-order species present under conditions for NMR (protein concentration of 500 $\mu$M). However, this GCAP1 dimerization appears only at protein concentrations above 100 $\mu$M (as judged by SEC analysis), and therefore, GCAP1 is monomeric at physiological concentrations in the rod cell (10−50 $\mu$M).

The HSQC spectrum of GCAP1 changed even further upon the addition of a saturating amount of $Ca^{2+}$ (Figure 5C). Spectral changes induced by the addition of a saturating amount of $Ca^{2+}$ to the $Mg^{2+}$-bound protein sample indicated that $Ca^{2+}$-induced conformational changes are distinct and separate from the $Mg^{2+}$-induced changes (Figure 5B,C). Three downfield-shifted peaks near 10.5 ppm are characteristic of conserved glycine residues at the 6-position of $Ca^{2+}$-occupied EF-hands (Gly69, Gly105, and Gly149), consistent with $Ca^{2+}$ bound at EF2, EF3, and EF4. Additional unique peaks of $Ca^{2+}$-bound GCAP1 (observed between 9 and 10 ppm) represent amino acid residues in EF3 and EF4 altered structurally by $Ca^{2+}$ binding. The HSQC spectrum of $Ca^{2+}$-saturated GCAP1 exhibited somewhat broadened peaks (like that of $Mg^{2+}$-bound protein) with variable NMR intensities, consistent with protein dimerization as measured by SEC. Pulsed-field gradient diffusion NMR studies determined a hydrodynamic radius of 3.8 nm, corresponding to a $Ca^{2+}$-bound protein dimer under NMR conditions.

The NMR peaks of $Ca^{2+}$-bound GCAP1 sharpened quite substantially upon addition of octyl glucoside detergent and with an increase in sample temperature to 47 °C (Figure 5D). Under these conditions, the protein became monomeric, which greatly improved the overall NMR sensitivity. Also, the chemical shifts remained unperturbed by the detergent, consistent with a monomeric and properly folded protein. Initially, this improvement in spectral quality suggested that it might be feasible to determine the full three-dimensional structure by NMR. However, upon closer inspection, we were able to identify only ~80% of the main chain amide resonances in HSQC spectra, and less than 50% of the resonances could be reliably assigned in triple-resonance experiments. The resonances with the strongest NMR intensities could be assigned mostly to residues in EF3 and EF4. However, many other resonances (associated with EF1 and EF2) had much weaker NMR intensities in triple-resonance experiments and could not be accurately assigned. Furthermore, the first 16 residues from the N-terminus and a stretch of ~20 residues following EF4 at the C-terminus have very weak NMR intensities due to exchange broadening as evidenced by their sharp temperature and magnetic-field dependence. These N- and C-terminal residues (italicized in Figure 1) are exchange-broadened more so for myristoylated GCAP1 compared to that of the unmyristoylated protein. Interestingly, many of these same residues are found in helices that interact with the myristoyl group in the X-ray structure. The exchange broadening for the N- and C-terminal residues suggests that these residues undergo dynamical motions on the chemical shift time scale to facilitate their interactions with the myristoyl group, and such dynamical behavior might be functionally important for recognition of RetGC.

*Myristoyl Group Structural Environment versus $Ca^{2+}$ and $Mg^{2+}$.* The recently published X-ray crystal structure of GCAP1 indicates that the myristoyl group is buried inside the $Ca^{2+}$-bound protein (*18*). This is in contrast to a solvent-exposed myristoyl group observed for GCAP2 (*43*), yeast frequenin (*38*), FCaBP (*44*), and recoverin (*20*). We performed NMR experiments on samples of apo, $Mg^{2+}$-bound, and $Ca^{2+}$-bound forms of GCAP1 with a covalently attached $^{13}C$-labeled myristoyl group to probe its structural environment inside the protein and to look for any effects of $Mg^{2+}$ or $Ca^{2+}$ binding. Previously, two-dimensional ($^{1}H-^{13}C$ HMQC) and three-dimensional ($^{13}C$-filtered NOESY-HMQC) NMR experiments on samples of recoverin that contained a $^{13}C$-labeled myristoyl group were used to selectively probe $Ca^{2+}$-induced changes to the chemical environment around the amino-terminal myristoyl group (*23, 32*). These studies revealed that the covalently attached fatty acyl chain in recoverin is sequestered in a hydrophobic pocket in the $Ca^{2+}$-free protein (*22*) and that binding of $Ca^{2+}$ leads to conformational changes that extrude the myristoyl group into solvent.

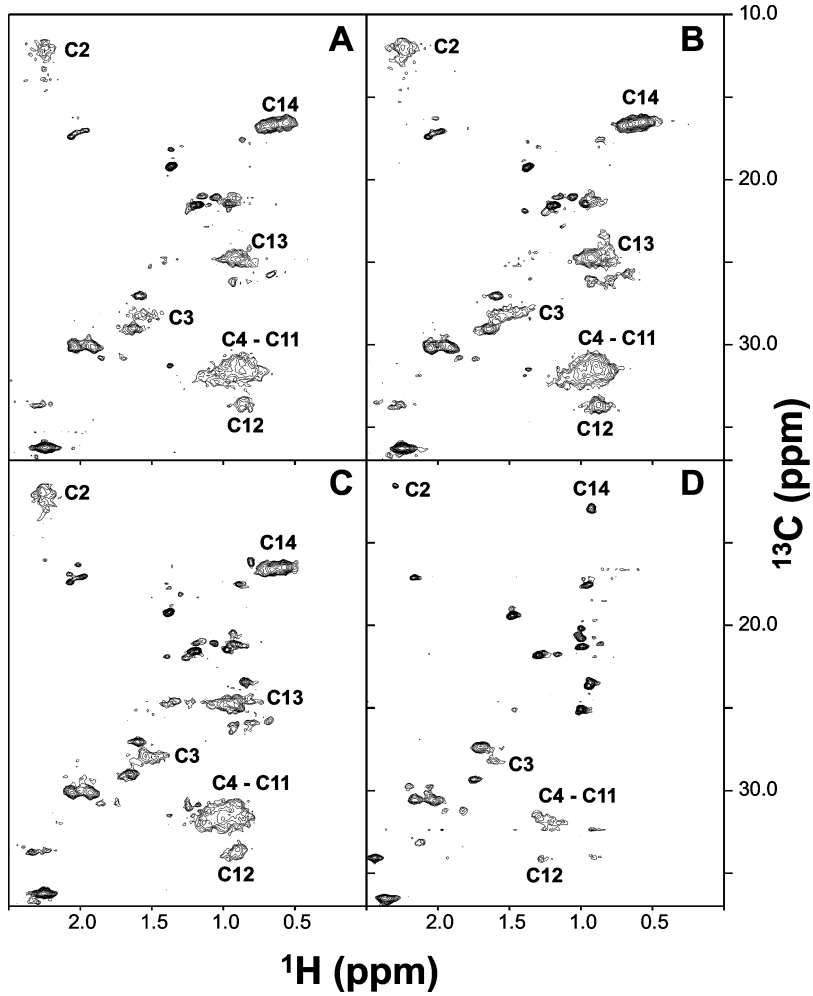


FIGURE 6: Two-dimensional $^{1}H-^{13}C$ HMQC NMR spectra of $^{13}C$-labeled myristoyl group attatched to unlabeled GCAP1 in the (A) $Ca^{2+}$-bound state, (B) $Mg^{2+}$-bound state, (C) apo state (1 mM EGTA), and (D) apo state in the presence of 8 M urea. The $^{13}C_2$ resonance of myristate is folded and aliased shown in the top left corner of the spectra. Extraneous peaks represent $^{13}C$ natural abundance signals from the protein as determined by recording $^{1}H-^{13}C$ HMQC spectra on GCAP1 samples with an unlabeled myristoyl group.

Similar NMR experiments were performed on samples of GCAP1 that contained a covalently attached $^{13}C$-labeled myristoyl group (Figure 6). Because the HMQC experiment selectively probes protons that are covalently attached to $^{13}C$, only the methylene and methyl resonances of the fatty acyl chain are expected to appear in these spectra. Extraneous peaks near 1.0, 1.4, 1.8, and 2.2 ppm ($^{1}H$ dimension) are due to background signals from the protein. The NMR spectrum of the myristoyl group of GCAP1 looks nearly identical for apo, $Mg^{2+}$-bound, and $Ca^{2+}$-bound forms of GCAP1 (Figure 6A−C), indicating that the structural environment around the myristoyl group does **not** depend on $Ca^{2+}$, in stark contrast to the large $Ca^{2+}$-induced spectral changes for the myristoyl group in recoverin (*20*).

The NMR chemical shifts of the myristoyl resonances of GCAP1 are consistent with the attached myristoyl group being sequestered inside a protein environment like that seen in the crystal structure (Table 3). Assignments of NMR resonances of the myristoyl group attached to GCAP1 were derived from assignments of free myristic acid in solution determined previously (*32*). The proton chemical shifts of the $C_{14}$ methyl (0.62−0.73 ppm) and $C_4-C_{12}$ methylene resonances (0.9−1.1 ppm) in GCAP1 are all somewhat upfield-shifted compared to the corresponding chemical shifts of free myristic acid in solution (*32*). These upfield chemical shifts in GCAP1 may be explained in part by aromatic groups (F39, F43, F63, and Y76) close the myristoyl group in the crystal structure that might impose an aromatic ring-current effect on the nearby myristoyl group. Indeed, the myristoyl group methyl and methylene proton chemical shifts in GCAP1 became downfield-shifted like those of myristate in solution when GCAP1 unfolded via addition of 8 M urea (Figure 6D and Table 3).

Table 3: $^{1}H$ ($^{13}C$) Chemical Shift Assignments of Myristoyl Resonances

| position | $Mg^{2+}$-GCAP1[a] | $Ca^{2+}$-GCAP1[b] | denatured GCAP1[c] |
|---|---|---|---|
| $C_2$ | 2.34 (38.5) | 2.34 (38.4) | 2.35 (38.2) |
| $C_3$ | 1.5 (27.8) | 1.5 (27.5) | 1.55 (27.0) |
| $C_4-C_{11}$ | 0.9−1.1 (31−33) | 0.9−1.1 (31−33) | 1.2−1.3 (32−33) |
| $C_{12}$ | 0.88 (34.0) | 0.92 (33.8) | 1.27 (33.5) |
| $C_{13}$ | 0.95 (24.4) | 0.98 (24.2) | 1.0 (25) |
| $C_{14}$ | 0.62, 0.73 (16.5) | 0.62, 0.73 (16.8) | 0.92 (13) |

[a] WIth NMR sample conditions of 0.3 mM GCAP1 in 5 mM Tris (pH 7.4) containing 5 mM $Mg^{2+}$. [b] WIth NMR sample conditions of 0.3 mM GCAP1 in 5 mM Tris (pH 7.4) containing 5 mM $Ca^{2+}$. [c] WIth NMR sample conditions of 0.3 mM GCAP1 in 5 mM Tris (pH 7.4) containing 8 M urea.

The spectral widths of the myristoyl NMR resonances in GCAP1 are strikingly broad (50−80 Hz) compared to the widths of the natural abundance protein peaks as well as the widths of myristoyl resonances in recoverin (*32*) and related

proteins (*38, 44*). The very broad NMR resonances of the myristoyl group in GCAP1 suggest that the attached myristoyl group may be located in a dynamic and/or heterogeneous protein environment. For free myristic acid in solution, a single proton resonance of the $C_{14}$ methyl group is quite sharp because free rotation of the methyl group about the $C_{13}-C_{14}$ single bond causes the three methyl protons to experience a time-averaged, uniform environment. By contrast, the $C_{14}$ methyl resonance ($^1$H dimension) in GCAP1 is quite broad and is partially split into two resolved components at 0.73 and 0.62 ppm with approximately equal intensity (Figure 6). This splitting (66 Hz) suggests that the $C_{14}$ methyl group may occupy at least two different structural environments. These two chemical shift environments represent distinct conformational states of the protein (e.g., activator vs inhibitor forms), but the relative intensities of the two components did not change much upon $Ca^{2+}$ binding. The two methyl resonances might also represent the myristoyl group in folded and misfolded protein forms or in two subunits of an asymmetric dimer. However, the spectral heterogeneity persisted in the presence of 25 mM octyl glucoside detergent (which causes GCAP1 to be monomeric), arguing against any artifacts caused by dimerization.

The apparent spectral heterogeneity and broadening imply that the myristoyl group must be in at least two different protein environments that are exchanging on the chemical shift time scale. The doublet methyl resonanace (66 Hz splitting) collapsed into a single broad peak (80 Hz line width) when the temperature was increased from 32 to 45 °C, consistent with an exchange rate on the millisecond time scale. The exchange behavior of the myristoyl resonances could also relate and help explain why the $^1$H$-^{15}$N HSQC peaks of the N- and C-terminal residues in GCAP1 (italicized in Figure 1) are exchange-broadened as described above (Figure 5). We propose that the N- and C-terminal residues, known to interact with the myristoyl group in the crystal structure (italicized in Figure 1), can undergo conformational fluctuations on the chemical shift time scale and therefore give rise to the spectral heterogeneity observed around the myristoyl $C_{14}$ methyl group.

To further probe the protein structural environment around the myristoyl group of GCAP1, three-dimensional ($^{13}$C/F$_1$)-edited and ($^{13}$C/F$_3$)-filtered NOESY experiments (*32*) were performed on unlabeled GCAP1 protein containing a $^{13}$C-labeled myristate. These spectra selectively probed atoms of residues in the protein that lie within 5 Å of the labeled $CH_3$ group of the myristoyl chain. Nuclear Overhauser effect (NOE) dipolar interactions between the myristate methyl group and the protein could not be detected (data not shown), because the exchange broadening of the methyl resonances described above severely attenuates any NOE signals. However, the myristate methylene resonances at $C_3$ and $C_4$ did exhibit detectable NOEs to aromatic protons from the protein (Figure 3 of the Supporting Information), providing further evidence that the myristoyl group is indeed surrounded by a hydrophobic and aromatic protein environment like what is observed in the crystal structure. The addition of $Ca^{2+}$ had no effect on the filtered NOESY spectrum, further confirming that the myristate remains sequestered in a protein environment in both $Ca^{2+}$-bound and $Ca^{2+}$-free GCAP1. This $Ca^{2+}$-independent sequestration of the myristate in GCAP1 is quite different from what is seen in recoverin that exhibits a sequestered myristoyl environment only in the $Ca^{2+}$-free protein (*20, 24*).

## DISCUSSION

In this study, we determined the energetics of $Mg^{2+}$ and $Ca^{2+}$ binding to GCAP1 as well as structural effects of myristoylation. $Ca^{2+}$ binds enthalpically to both EF3 and EF4 in the nanomolar range with more than 1000-fold selectivity over $Mg^{2+}$. EF2 binds entropically to both $Ca^{2+}$ and $Mg^{2+}$ and undergoes metal-induced conformational changes related to cyclase regulation (*17*). Myristoylation has almost no influence on the $Ca^{2+}$ and $Mg^{2+}$ binding properties of GCAP1. Furthermore, the $Ca^{2+}$-induced structural changes in the EF-hands do not influence the structural environment that surrounds the sequestered myristoyl group. Unlike recoverin, the myristoyl group attached to GCAP1 remains buried inside the protein regardless of $Ca^{2+}$ level, and GCAP1 does **not** possess a functional $Ca^{2+}$-myristoyl switch.

The $Ca^{2+}$ dissociation constants ($K_{EF2}$, $K_{EF3}$, and $K_{EF4}$) of wild-type GCAP1 are somewhat different from those of the mutants (Table 1), implying that the three $Ca^{2+}$-binding sites must interact and possess some cooperativity. Indeed, the EF3− mutation in GCAP1 abolishes $Ca^{2+}$ binding to EF4 (*16*), suggesting both ordered and cooperative $Ca^{2+}$ binding at EF3 and EF4. In essence, $Ca^{2+}$ must bind at EF3 first to facilitate subsequent binding at EF4. Such ordered $Ca^{2+}$ binding is consistent with our measurement that EF3 has the highest binding affinity ($K_{EF3} = 80$ nM), whereas EF4 has the intermediate affinity ($K_{EF4} = 200$ nM) and EF2 the lowest affinity ($K_{EF2} = 0.9\ \mu$M). Cooperative $Ca^{2+}$ binding between EF3 and EF4 is also consistent with their intimate structural contacts observed in the X-ray crystal structure (*18*), and concerted $Ca^{2+}$-induced NMR spectral changes observed for Gly105 (EF3) and Gly149 (EF4) in Figure 4 of the Supporting Information. This cooperativity seems at odds with the overall $Ca^{2+}$ binding isotherm of GCAP1 having a Hill slope of 1.0 (*16*). The Hill coefficient in this case, however, is not always a reliable measure of cooperativity, particularly if the individual sites have different intrinsic affinities (*45*). The free energy of interaction between the two sites ($\Delta G_{interact}$) is a more stringent definition of cooperativity, and this interaction energy can be inferred by comparing how the dissociation constant of EF3 [$K_{EF3} = \exp(-\Delta G°/RT)$] changes when EF4 is disabled (EF4−). For GCAP1, $K_{EF3}$ increases subtantially by disabling EF4 (Table 1), which means that $\Delta G_{interact} > 0$ and the two sites have positive cooperativity. We propose that this positive cooperativity of $Ca^{2+}$ binding between EF3 and EF4 could help explain how GCAP1 confers such a steep $Ca^{2+}$-dependent activation of RetGC with a Hill coefficient of 2 (*46*). The cooperative cyclase activation may also arise in part by $Ca^{2+}$-induced dimerization of RetGC (*47*).

The results of this study provide structural insights into the regulatory mechanism of RetGC. The activation of RetGC by $Ca^{2+}$-free GCAP1 requires physiological $Mg^{2+}$ levels (*16*). Our NMR structural analysis shows that the completely metal-free (apo) GCAP1 lacks organized tertiary structure, explaining why the apo state is physiologically inactive (Figure 5A). $Mg^{2+}$ binding induces structural changes in the EF-hands and stabilizes protein tertiary structure as evidenced by DSC (Figure 4) and NMR (Figure 5). $Mg^{2+}$

binds most tightly to GCAP1 at EF2 (Table 2), which we suggest might constitute an important interaction site for cyclase activation. Indeed, recent biochemical and cell biology studies have shown that EF2 is required for the cyclase interaction (*12, 17*) and promotes docking of $Mg^{2+}$-bound GCAP1 on RetGC (*17*). In addition, $Mg^{2+}$ binding at EF3 appears to facilitate the docking of GCAP1 with RetGC, because cyclase binding to GCAP1 is weakened by a mutation that blocks $Mg^{2+}$ binding at EF3 (*12*). Finally, $Ca^{2+}$ binding at EF4 is necessary and sufficient for GCAP1 to inhibit RetGC when the $Ca^{2+}$ concentration increases in the dark (*12, 16*). It seems likely that $Ca^{2+}$ binding at EF4 may promote the docking of $Ca^{2+}$-bound GCAP1 to the cyclase (*48, 49*).

The replacement of bound $Ca^{2+}$ with $Mg^{2+}$ in GCAP1 is functionally important for switching GCAP1 from a $Ca^{2+}$-bound inhibitor to a $Mg^{2+}$-bound activator conformational state during light activation. The relatively low apparent $Ca^{2+}$ binding affinity of EF2 measured by ITC is explained by its thermodynamic coupling to an unfavorable protein conformational change probed structurally by NMR (Figure 5). The intrinsic $Ca^{2+}$ binding to EF2 measured by a direct $Ca^{2+}$ binding assay ($K_a = 10^7\ M^{-1}$) coupled to an unfavorable conformational change ($K_{eq} \sim 10^{-1}$) yields an overall binding constant of $K_{tot}$ ($=K_aK_{eq} \sim 10^6\ M^{-1}$), consistent with the overall $K_{EF2}$ measured by ITC. Thus, the intrinsic $Ca^{2+}$ binding constants inferred from the ITC analysis are consistent with those measured by direct equilibrium binding assays (*16*) and consistent with the functional behavior of GCAP1 in physiological analyses (*16, 17*). The relative binding affinities of $Mg^{2+}$ ($K_{EF2} = 0.7$ mM) and $Ca^{2+}$ ($K_{EF2} = 0.9\ \mu$M) at EF2 suggest that a fraction of GCAP1 will be occupied with $Mg^{2+}$ even in dark-adapted rods [250 nM $Ca^{2+}$ and 1 mM $Mg^{2+}$ (*35*)], and virtually all of the EF2 sites are occupied by $Mg^{2+}$ upon illumination, when the $Ca^{2+}$ concentration decreases below 100 nM (*50*). For EF3 and EF4, the relatively weak $Mg^{2+}$ binding ($K_d = 2$ mM) and strong $Ca^{2+}$ binding ($K_{EF3} = 80$ nM, and $K_{EF4} = 200$ nM) mean that both of these sites are fully occupied by $Ca^{2+}$ in the dark. $Mg^{2+}$ can bind to these sites only under bright light illumination, when the free $Ca^{2+}$ concentration in rod outer segment falls drastically to ~25 nM (*50*). $Mg^{2+}$ binding at EF3 is required for RetGC activation (*12, 16, 17*), whereas $Mg^{2+}$ binding at EF4 is not essential (*12, 16*), suggesting that EF4 does not bind functionally to $Mg^{2+}$.

$Ca^{2+}$ binding to GCAP1 leads to protein conformational changes that cause inhibition of RetGC activity at high $Ca^{2+}$ levels in the rod cell, which is necessary for the maintenance of a steady cGMP level in the dark that otherwise may lead to retinal disease (*8, 51*). Our ITC and NMR studies suggest that GCAP1 binds cooperatively to $Ca^{2+}$ at EF3 and EF4 that promotes a $Ca^{2+}$-induced conformational change (Figure 5). Indeed, a number of residues in EF3 and EF4 (e.g., Gly105 and Gly149) exhibit $Ca^{2+}$-induced NMR spectral changes that occur in a concerted fashion (Figure 4 of the Supporting Information). Also, binding of $Ca^{2+}$ at EF3 and EF4 displays in each case large negative $\Delta C_p$ values (−379 and −101 cal $mol^{-1}\ K^{-1}$, respectively), suggesting that $Ca^{2+}$ binding at both sites promotes an overall burial of hydrophobic residues (*29*). This seems somewhat at odds with $Ca^{2+}$-dependent changes in intrinsic Trp fluorescence from GCAP1, especially for Trp21 in EF1 and Trp94 in EF3 (*46, 52*). Trp21 and Trp94 shift into polar environments in both the $Mg^{2+}$-bound and $Ca^{2+}$-bound GCAP1 relative to its apo conformation, whereas Trp94 shifts back into a more hydrophobic environment when $Ca^{2+}$ replaces $Mg^{2+}$ at EF3 (*16*). Our ITC analysis detects an overall $Ca^{2+}$-induced decrease in exposed hydrophobic surface area, because ITC detects signals from all residues of the protein (and not just Trp). Therefore, $Ca^{2+}$ binding at EF3 and EF4 causes conformational changes leading to a net burial of hydrophobic residues in GCAP1 that presumably compensates for the exposure of Trp21 and Trp94.

What is the structural and functional role of the N-terminal myristoyl group of GCAP1? Myristoylation of GCAP1 is thought to be important for the regulation of RetGC (*53, 54*), and the recently determined crystal structure of GCAP1 shows the myristate to be buried inside the protein hydrophobic core (*18*). In this study, our NMR analyses confirmed that the myristoyl group in GCAP1 is indeed sequestered inside a protein environment in the native conformation of the protein in solution. Upfield chemical shifts and NOE patterns of the myristoyl resonances (Figure 6 and Table 3) are consistent with ring currents imposed by aromatic residues (F39, F43, F63, and Y76) shown to be near the myristate in the crystal structure. $Ca^{2+}$ and/or $Mg^{2+}$ binding to GCAP1 has very little influence on the chemical shifts and NOE patterns of the myristoyl group (Figure 6), suggesting that the myristoyl group remains in a similar environment in both the $Mg^{2+}$-bound activator and $Ca^{2+}$-bound inhibitor forms of GCAP1. Surprisingly, however, myristoylation of GCAP1 has only a small effect on the overall protein folding stability (Figure 4) and structure of the EF-hands (Figure 5). Thus, it seems that myristoylation interacts most strongly with residues outside the EF-hand regions, namely, the N- and C-terminal helices that contact the myristate in the crystal structure (italicized in Figure 1). Interestingly, the NMR resonances of these N- and C-terminal residues and those of myristate are all spectrally quite broad (line width, $\Delta\nu = 50-80$ Hz) due to exchange processes on the millisecond time scale ($\tau_{ex} \propto 1/\Delta\nu$), suggesting a highly dynamic environment around the myristate. These millisecond exchange processes (activation energy of ~30 kJ/mol) occur at physiological temperatures but are essentially frozen out under conditions for X-ray crystallography (77 K), explaining why this dynamical behavior apparently was not observed in the crystal structure. We propose that conformational fluctuations at the myristoyl binding site might regulate the cyclase by enabling specific recognition of RetGC or by facilitating secondary interactions required for RetGC activation.

## ACKNOWLEDGMENT

We are grateful to Dr. Jeff de Ropp for help with NMR experiments, Dr. Frits Abildgaard for providing NMR pulse sequence programs, and Frank Delaglio for writing computer software for NMR data processing and analysis.

## SUPPORTING INFORMATION AVAILABLE

Summary of DSC data of myristoylated and unmyristoylated recoverin, fluorescence spectra of myristoylated and unmyristoylted GCAP1, $^{13}C(F3)$-filtered and $^{13}C(F1)$-edited NOESY-HMQC spectrum of GCAP1 containing a $^{13}C$-labeled myristoyl group, and a plot of the relative NMR

intensities of amide $^1$H resonances from Gly105 (EF3) and Gly149 (EF4) versus $Ca^{2+}$. This material is available free of charge via the Internet at http://pubs.acs.org.

## REFERENCES


1. Burgoyne, R. D. (2007) Neuronal calcium sensor proteins: Generating diversity in neuronal $Ca^{2+}$ signalling. *Nat. Rev. Neurosci. 8*, 182–193.
2. Burgoyne, R. D., and Weiss, J. L. (2001) The neuronal calcium sensor family of $Ca^{2+}$-binding proteins. *Biochem. J. 353*, 1–12.
3. Ames, J. B., Tanaka, T., Stryer, L., and Ikura, M. (1996) Portrait of a myristoyl switch protein. *Curr. Opin. Struct. Biol. 6*, 432–438.
4. Dizhoor, A. M., Lowe, D. G., Olsevskaya, E. V., Laura, R. P., and Hurley, J. B. (1994) The human photoreceptor membrane guanylyl cyclase, RetGC, is present in outer segments and is regulated by calcium and a soluble activator. *Neuron 12*, 1345–1352.
5. Palczewski, K., Subbaraya, I., Gorczyca, W. A., Helekar, B. S., Ruiz, C. C., Ohguro, H., Huang, J., Zhao, X., Crabb, J. W., and Johnson, R. S. (1994) Molecular cloning and characterization of retinal photoreceptor guanylyl cyclase-activating protein. *Neuron 13*, 395–404.
6. Palczewski, K., Polans, A. S., Baehr, W., and Ames, J. B. (2000) $Ca^{2+}$-binding proteins in the retina: Structure, function, and the etiology of human visual diseases. *BioEssays 22*, 337–350.
7. Stephen, R., Filipek, S., Palczewski, K., and Sousa, M. C. (2008) $Ca^{2+}$-dependent regulation of phototransduction. *Photochem. Photobiol. 84*, 903–910.
8. Payne, A. M., Downes, S. M., Bessant, D. A., Taylor, R., Holder, G. E., Warren, M. J., Bird, A. C., and Bhattacharya, S. S. (1998) A mutation in guanylate cyclase activator 1A (GUCA1A) in an autosomal dominant cone dystrophy pedigree mapping to a new locus on chromosome 6p21.1. *Hum. Mol. Genet. 7*, 273–277.
9. Baylor, D. (1996) How photons start vision. *Proc. Natl. Acad. Sci. U.S.A. 93*, 560–565.
10. Koch, K. W., and Stryer, L. (1988) Highly cooperative feedback control of retinal rod guanylate cyclase by calcium ions. *Nature 334*, 64–66.
11. Olshevskaya, E. V., Calvert, P. D., Woodruff, M. L., Peshenko, I. V., Savchenko, A. B., Makino, C. L., Ho, Y. S., Fain, G. L., and Dizhoor, A. M. (2004) The Y99C mutation in guanylyl cyclase-activating protein 1 increases intracellular $Ca^{2+}$ and causes photoreceptor degeneration in transgenic mice. *J. Neurosci. 24*, 6078–6085.
12. Peshenko, I. V., and Dizhoor, A. M. (2007) Activation and inhibition of photoreceptor guanylyl cyclase by guanylyl cyclase activating protein 1 (GCAP-1): The functional role of $Mg^{2+}$/$Ca^{2+}$ exchange in EF-hand domains. *J. Biol. Chem. 282*, 21645–21652.
13. Dizhoor, A. M., Olshevskaya, E. V., Henzel, W. J., Wong, S. C., Stults, J. T., Ankoudinova, I., and Hurley, J. B. (1995) Cloning, sequencing and expression of a 24-kDa $Ca^{2+}$-binding protein activating photoreceptor guanylyl cyclase. *J. Biol. Chem. 270*, 25200–25206.
14. Imanishi, Y., Li, N., Sokal, I., Sowa, M. E., Lichtarge, O., Wensel, T. G., Saperstein, D. A., Baehr, W., and Palczewski, K. (2002) Characterization of retinal guanylate cyclase-activating protein 3 (GCAP3) from zebrafish to man. *Eur. J. Neurosci. 15*, 63–78.
15. Imanishi, Y., Yang, L., Sokal, I., Filipek, S., Palczewski, K., and Baehr, W. (2004) Diversity of guanylate cyclase-activating proteins (GCAPs) in teleost fish: Characterization of three novel GCAPs (GCAP4, GCAP5, GCAP7) from zebrafish (*Danio rerio*) and prediction of eight GCAPs (GCAP1−8) in pufferfish (*Fugu rubripes*). *J. Mol. Evol. 59*, 204–217.
16. Peshenko, I. V., and Dizhoor, A. M. (2006) $Ca^{2+}$ and $Mg^{2+}$ binding properties of GCAP-1. Evidence that $Mg^{2+}$-bound form is the physiological activator of photoreceptor guanylyl cyclase. *J. Biol. Chem. 281*, 23830–23841.
17. Peshenko, I. V., Olshevskaya, E. V., and Dizhoor, A. M. (2008) Binding of guanylyl cyclase activating protein 1 (GCAP1) to retinal guanylyl cyclase (RetGC1). The role of individual EF-hands. *J. Biol. Chem. 283*, 21747–21757.
18. Stephen, R., Bereta, G., Golczak, M., Palczewski, K., and Sousa, M. C. (2007) Stabilizing function for myristoyl group revealed by the crystal structure of a neuronal calcium sensor, guanylate cyclase-activating protein 1. *Structure 15*, 1392–1402.
19. Ames, J. B., Dizhoor, A. M., Ikura, M., Palczewski, K., and Stryer, L. (1999) Three-dimensional structure of guanylyl cyclase activating protein-2, a calcium-sensitive modulator of photoreceptor guanylyl cyclases. *J. Biol. Chem. 274*, 19329–19337.
20. Ames, J. B., Ishima, R., Tanaka, T., Gordon, J. I., Stryer, L., and Ikura, M. (1997) Molecular mechanics of calcium-myristoyl switches. *Nature 389*, 198–202.
21. Ames, J. B., Ikura, M., and Stryer, L. (2000) Molecular structure of membrane-targeting calcium sensors in vision: Recoverin and guanylate cyclase-activating protein 2. *Methods Enzymol. 316*, 121–132.
22. Tanaka, T., Ames, J. B., Harvey, T. S., Stryer, L., and Ikura, M. (1995) Sequestration of the membrane-targeting myristoyl group of recoverin in the calcium-free state. *Nature 376*, 444–447.
23. Tanaka, T., Ames, J. B., Kainosho, M., Stryer, L., and Ikura, M. (1998) Differential isotype labeling strategy for determining the structure of myristoylated recoverin by NMR spectroscopy. *J. Biomol. NMR 11*, 135–152.
24. Valentine, K., Mesleh, M., Ikura, M., Ames, J. B., and Opella, S. (2003) Structure, topology and dynamics of myristoylated recoverin bound to phospholipid bilayers. *Biochemistry 42*, 6333–6340.
25. Osawa, M., Dace, A., Tong, K. I., Valiveti, A., Ikura, M., and Ames, J. B. (2005) $Mg^{2+}$ and $Ca^{2+}$ differentially regulate DNA binding and dimerization of DREAM. *J. Biol. Chem. 280*, 18008–18014.
26. Ames, J. B., Hamasaki, N., and Molchanova, T. (2002) Structure and calcium-binding studies of a recoverin mutant (E85Q) in an allosteric intermediate state. *Biochemistry 41*, 5776–5787.
27. Tsien, R. Y. (1989) A new generation of $Ca^{2+}$ indicators with greatly improved fluorescence properties. *Methods Cell Biol. 30*, 127–156.
28. Wingard, J. N., Chan, J., Bosanac, I., Haeseleer, F., Palczewski, K., Ikura, M., and Ames, J. B. (2005) Structural analysis of $Mg^{2+}$ and $Ca^{2+}$ binding to CaBP1, a neuron-specific regulator of calcium channels. *J. Biol. Chem. 280*, 37461–37470.
29. Gomez, J., Hilser, V. J., Xie, D., and Freier, E. (1995) The heat capacity of proteins. *Proteins 22*, 404–412.
30. Gomez, J., and Freier, E. (1995) Thermodynamic mapping of the inhibitor site of the aspartic protease endothiapepsin. *J. Mol. Biol. 252*, 337–350.
31. Wiseman, T., Williston, S., Brandts, J. F., and Lin, L. N. (1989) Rapid measurement of binding constants and heats of binding using a new titration calorimeter. *Anal. Biochem. 179*, 131–137.
32. Ames, J. B., Tanaka, T., Ikura, M., and Stryer, L. (1995) Nuclear magnetic resonance evidence for $Ca^{2+}$-induced extrusion of the myristoyl group of recoverin. *J. Biol. Chem. 270*, 30909–30913.
33. Ames, J. B., Porumb, T., Tanaka, T., Ikura, M., and Stryer, L. (1995) Amino-terminal myristoylation induces cooperative calcium binding to recoverin. *J. Biol. Chem. 270*, 4526–4533.
34. Maune, J. F., Klee, C. B., and Beckingham, K. (1992) $Ca^{2+}$ binding and conformational change in two series of point mutations to the individual $Ca^{2+}$-binding sites of calmodulin. *J. Biol. Chem. 267*, 5286–5295.
35. Chen, C., Nakatani, K., and Koutalos, Y. (2003) Free magnesium concentration in salamander photoreceptor outer segments. *J. Physiol. 553*, 125–135.
36. Flaherty, K. M., Zozulya, S., Stryer, L., and McKay, D. B. (1993) Three-dimensional Structure of Recoverin, a Calcium Sensor in Vision. *Cell 75*, 709–716.
37. Zhou, W., Qian, Y., Kunjilwar, K., Pfaffinger, P. J., and Choe, S. (2004) Structural insights into the functional interaction of KChIP1 with Shal-type $K^+$ channels. *Neuron 41*, 573–586.
38. Ames, J. B., Hendricks, K. B., Strahl, T., Huttner, I. G., Hamasaki, N., and Thorner, J. (2000) Structure and calcium-binding properties of Frq1, a novel calcium sensor in the yeast *Saccharomyces cerevisiae*. *Biochemistry 39*, 12149–12161.
39. Yamniuk, A. P., Nguyen, L. T., Hoang, T. T., and Vogel, H. J. (2004) Metal ion binding properties and conformational states of calcium- and integrin-binding protein. *Biochemistry 43*, 2558–2568.
40. Gombos, Z., Durussel, I., Ikura, M., Rose, D. R., Cox, J. A., and Chakrabarti, A. (2003) Conformational coupling of $Mg^{2+}$ and $Ca^{2+}$ on the three-state folding of calexcitin B. *Biochemistry 42*, 5531–5539.
41. Qi, X. F., Bagby, S., Gombos, Z., Ikura, M., and Chakrabarti, A. (2001) Alternate routes to conformational specificity in a Greek key $\beta$ barrel protein. *Eur. J. Biochem. 268*, 4653–4663.
42. Altieri, A. S., Hinton, D. P., and Byrd, R. A. (1995) Association of biomolecular systems via pulsed field gradient NMR self-diffusion measurements. *J. Am. Chem. Soc. 117*, 7566–7567.

43. Vogel, A., Schroder, T., Lange, C., and Huster, D. (2007) Characterization of the myristoyl lipid modification of membrane-bound GCAP-2 by $^2$H solid-state NMR spectroscopy. *Biochim. Biophys. Acta 1768*, 3171–3181.
44. Wingard, J. N., Ladner, J., Vanarotti, M., Fisher, A. J., Buchanan, K. T., Engman, D. M., and Ames, J. B. (2008) Structural insights into membrane targeting by the flagellar calcium-binding protein (FCaBP), a myristoylated and palmitoylated calcium sensor in *Trypanosoma cruzi*. *J. Biol. Chem. 283*, 23388–23396.
45. Forsen, S., and Linse, S. (1995) Cooperativity: Over the Hill. *Trends Biochem. Sci. 20*, 495–497.
46. Peshenko, I. V., and Dizhoor, A. M. (2004) Guanylyl cyclase-activating proteins (GCAPs) are $Ca^{2+}/Mg^{2+}$ sensors: Implications for photoreceptor guanylyl cyclase (RetGC) regulation in mammalian photoreceptors. *J. Biol. Chem. 279*, 16903–16906.
47. Ramamurthy, V., Tucker, C., Wilkie, S. E., Daggett, V., Hunt, D. M., and Hurley, J. B. (2001) Interactions within the coiled-coil domain of RetGC-1 guanylyl cyclase are optimized for regulation rather than for high affinity. *J. Biol. Chem. 276*, 26218–26229.
48. Dizhoor, A. M., Boikov, S. G., and Olshevskaya, E. V. (1998) Constitutive activation of photoreceptor guanylate cyclase by Y99C mutant of GCAP-1. Possible role in causing human autosomal dominant cone degeneration. *J. Biol. Chem. 273*, 17311–17314.
49. Krylov, D. M., Niemi, G. A., Dizhoor, A. M., and Hurley, J. B. (1999) Mapping sites in guanylyl cyclase activating protein-1 required for regulation of photoreceptor membrane guanylyl cyclases. *J. Biol. Chem. 274*, 10833–10839.
50. Woodruff, M. L., Sampath, A. P., Mathews, H. R., Krasnoperova, N. V., Lem, J., and Fain, G. L. (2002) Measurement of cytoplasmic calcium concentration in the rods of wild-type and transducin knock-out mice. *J. Physiol. 542*, 843–854.
51. Woodruff, M. L., Janisch, K. M., Peshenko, I. V., Dizhoor, A. M., Tsang, S. H., and Fain, G. L. (2008) Modulation of phosphodiesterase6 turnoff during background illumination in mouse rod photoreceptors. *J. Neurosci. 28*, 2064–2074.
52. Sokal, I., Otto-Bruc, A. E., Surgucheva, I., Verlinde, C. L., Wang, C. K., Baehr, W., and Palczewski, K. (1999) Conformational changes in guanylyl cyclase-activating protein 1 (GCAP1) and its tryptophan mutants as a function of calcium concentration. *J. Biol. Chem. 274*, 19829–19837.
53. Hwang, J. Y., and Koch, K. W. (2002) Calcium- and myristoyl-dependent properties of guanylate cyclase-activating protein-1 and protein-2. *Biochemistry 41*, 13021–13028.
54. Hwang, J. Y., Lange, C., Helten, A., Hoppner, D., Duda, T., Sharma, R. K., and Koch, K. W. (2003) Regulatory modes of rod outer segment membrane guanylate cyclase differ in catalytic efficiency and $Ca^{2+}$-sensitivity. *Eur. J. Biochem. 270*, 3814–3821.

BI801897P